Effect of Fiber Waviness on the Nonlinear Elastic Behavior of Flexible Composites

CHEN-MING KUO
Division of Applied Mechanics
Department of Mechanical Engineering
Stanford University
Stanford, California 94305, U.S.A.

KIYOHISA TAKAHASHI
Department of Materials Science and Engineering
Nagoya Institute of Technology
Gokiso-cho
Showa-Ku, Nagoya 466, Japan

TSU-WEI CHOU
Department of Mechanical Engineering
Center for Composite Materials
University of Delaware
Newark, Delaware 19716, U.S.A.

(Received October 9, 1987)
(Revised February 7, 1988)

ABSTRACT

The effect of fiber waviness on the elastic moduli of flexible composites is investigated theoretically and experimentally. The flexible composites examined are composed of continuous fibers with sinusoidal waviness in an elastomeric matrix. Both iso-phase and random-phase fiber arrangements are used for this study. The constitutive relations for the longitudinal and transverse tensile behavior have been developed for these models. Tensile tests have been conducted to verify the constitutive relations. Carbon fiber and silicone elastomer were used for the experiments. Techniques for specimen fabrication as well as photoelastic tests are also presented. Experimental results show good agreement with the theoretical predictions.

1. INTRODUCTION

IN A RECENT review article [1], Chou, McCullough and Pipes discussed the versatility of fiber composite material applications. The unique characteristic of

0021-9983/88/11 1004–22 $4.50/0

composites stems from our ability to tailor the microstructure to achieve specific material performance. One example of such design of microstructure cited in Reference [1] concerns the large nonlinear deformation of flexible composites originally proposed by Chou and Luo [2,3]. To understand the background of development of flexible composite, it is necessary to recall the relationship between flexible composites and textile composites.

The structures and properties of two-dimensional and three-dimensional textile composites have been investigated by Chou and co-workers [4–10] in a series of publications. One of the major findings is that the fiber undulation leads to a reduction in the in-plane stiffness and enhances the nonlinear behavior of textile composites. The nonlinear behavior due to fiber undulation was first examined by Ishikawa and Chou [7]. In their study, the matrices are conventional thermosetting resin materials. Due to the low deformability of the matrices, the nonlinear behavior is not very significant although there exist the fiber crimped regions in the textile preforms. This phenomenon provided the motivation for exploring the effect of fiber waviness on composite behavior. A flexible composite system is used for this purpose.

As defined by Chou, Luo and Takahashi [2,3,11], flexible composites are elastomeric polymer based composites for which the usable range of deformation is much larger than that of the conventional thermosetting or thermoplastic polymer based composites. In order to sustain large deformation, the fibers must be able to deform with the matrix. They suggested the use of fibers with sinusoidal waviness in order to enhance the extensibility of composites. Due to the undulating fibers embedded in an elastomeric matrix, flexible composites can elongate readily at low stresses but stiffen when the fibers become fully extended. Two types of fiber arrangement, iso-phase and random-phase models, have been proposed and the longitudinal tensile behavior of flexible composites based on these models has been examined [11].

Chou and Takahashi [11] examined the longitudinal tensile behavior of flexible composites from an analytical viewpoint for iso-phase and random-phase models. Their theoretical predictions are based upon a step-wise incremental method and the laminated plate theory. Treatment of the nonlinear elastic behavior of flexible composites from the viewpoint of finite elasticity has been performed by Luo and Chou [12]. Reports of specimen fabrications and experimental methods can be found in References [2,3, 12 and 13]. However, no analysis was made on specimens with wavy fibers under transverse tension in Reference [12].

In order to further understand the fundamental characteristics of flexible composites, the transverse elastic behavior is analyzed and experimental studies are reported in this paper. The nonlinear elastic constitutive relations for transverse tensile behavior of both iso-phase and random-phase models are developed in Sections 3.2 and 4.2. The materials, fabrication method and experiments are given in Section 5. Finally, comparisons between theoretical predictions and experimental data are presented in Section 6. In order to provide the necessary analytical background, Sections 2, 3.1 and 4.1 recapitulate the work of Chou and Takahashi [11].

2. CURVED FIBER

Following Chou and Takahashi [11] the spatial position of a typical wavy fiber in the xyz coordinates is given by

$$y = a \sin \frac{2\pi x}{\lambda} \tag{1}$$

where a and λ are the amplitude and wavelength of the curved fiber, respectively (Figure 1). The angle (θ) between the tangent to the fiber and x axis is a function of x.

$$\tan \theta = \frac{dy}{dx} = \frac{2\pi a}{\lambda} \cos \frac{2\pi x}{\lambda} \tag{2}$$

Obviously, the maximum value of tan θ occurs at

$$\theta_{max} = \tan^{-1}\left(\frac{2\pi a}{\lambda}\right) \tag{3}$$

The fiber length, s, between $x = 0$ and λ is obtained by integrating through one

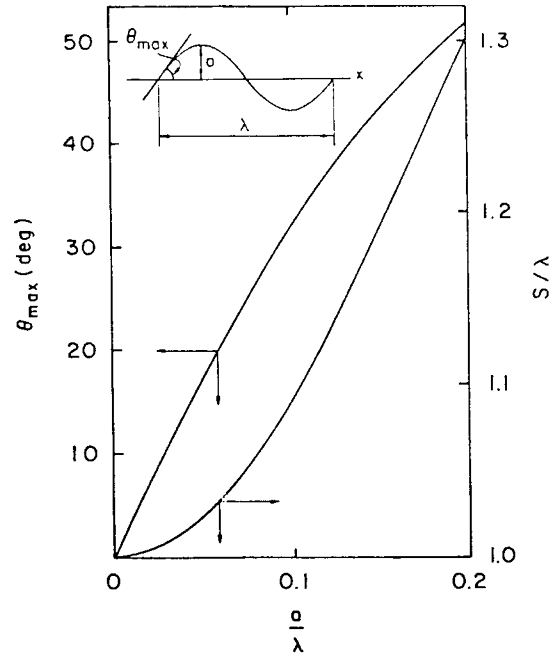

***Figure 1.** Geometrical relations among a/λ, s/λ and θ_{max} [11].*

wavelength and using the second kind of elliptic integral and Taylor expansion [11].

$$\frac{s}{\lambda} = 1 + 2\left(\frac{k^2}{8}\right) + 13\left(\frac{k^2}{8}\right)^2 + 90\left(\frac{k^2}{8}\right)^3 + 644\left(\frac{k^2}{8}\right)^4 + 4708.5\left(\frac{k^2}{8}\right)^5 + \ldots \tag{4}$$

where

$$k^2 = \frac{c}{1 + c}; \qquad c = \left(\frac{2\pi a}{\lambda}\right)^2 \tag{5}$$

The relations between θ_{max}, s/λ and a/λ are also shown in Figure 1.

3. ISO-PHASE MODEL

The iso-phase model [11] is depicted in Figure 2; all the fibers are in the same phase along the x direction. Each small volume element of the composite between x and $x + dx$ is approximated by a unidirectional fiber composite, in which fibers are inclined at an angle θ to the x axis, as defined by Equation (2). Based upon this assumption, the two-dimensional lamina theory [14] can be applied as follows.

The constitutive relations for an off-axis unidirectional lamina with fiber orientation θ in the xy plane are given by [14]

$$\begin{Bmatrix} e_x \\ e_y \\ \gamma_{xy} \end{Bmatrix} = \begin{bmatrix} \bar{S}_{11} & \bar{S}_{12} & \bar{S}_{16} \\ \bar{S}_{12} & \bar{S}_{22} & \bar{S}_{26} \\ \bar{S}_{16} & \bar{S}_{26} & \bar{S}_{66} \end{bmatrix} \begin{Bmatrix} \sigma_x \\ \sigma_y \\ \tau_{xy} \end{Bmatrix} \tag{6}$$

where

$$\begin{aligned}
\bar{S}_{11} &= S_{11}\cos^4\theta + S_{22}\sin^4\theta + (2S_{12} + S_{66})\sin^2\theta\cos^2\theta \\
\bar{S}_{12} &= S_{12} + (S_{11} - 2S_{12} + S_{22} - S_{66})\sin^2\theta\cos^2\theta \\
\bar{S}_{22} &= S_{11}\sin^4\theta + S_{22}\cos^4\theta + (2S_{12} + S_{66})\sin^2\theta\cos^2\theta \\
\bar{S}_{16} &= (2S_{11} - 2S_{12} - S_{66})\cos^3\theta\sin\theta + (2S_{12} - 2S_{22} + S_{66})\cos\theta\sin^3\theta \\
\bar{S}_{26} &= (2S_{11} - 2S_{12} - S_{66})\cos\theta\sin^3\theta + (2S_{12} - 2S_{22} + S_{66})\cos^3\theta\sin\theta \\
\bar{S}_{66} &= 4(S_{11} - 2S_{12} + S_{22} - S_{66})\sin^2\theta\cos^2\theta + S_{66}
\end{aligned} \tag{7}$$

S_{11}, S_{22}, S_{12} and S_{66} are the elastic compliances of the unidirectional lamina. The stretching-shear coupling is represented by $\bar{S}_{16}$ and $\bar{S}_{26}$ in Equations (6) and (7).

In a small volume element between x and $x + dx$, the tensile strain along the

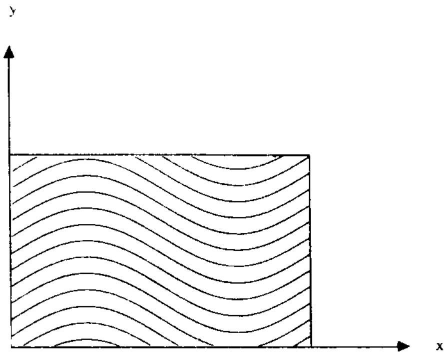

Figure 2. *Iso-phase model [11].*

fibers is expressed by

$$e_L = e_x \cos^2\theta + e_y \sin^2\theta + \gamma_{xy} \sin\theta \cos\theta \tag{8}$$

3.1 Longitudinal Modulus

The effective Young's modulus of the iso-phase model in the x direction is obtained by Chou and Takahashi [11].

$$E_x^* = \frac{(1+c)^{3/2}}{\left(1+\frac{c}{2}\right)S_{11} - \left[1+\frac{3}{2}c - (1+c)^{3/2}\right]S_{22} + \frac{c}{2}(2S_{12}+S_{66})} \tag{9}$$

And, the average tensile strain along the fibers is given by [11]

$$\bar{e}_L = \{(S_{11} - S_{12})F(k) + S_{12}\}\,\sigma_x \tag{10}$$

where

$$F(k) \approx 1 - \frac{1}{2}k^2 - \frac{3}{16}k^4 - \frac{3}{32}k^6 - \frac{111}{2048}k^8 - \frac{141}{4096}k^{10} \tag{11}$$

3.2 Transverse Modulus

Two approaches have been adopted for analyzing the transverse tensile behavior, namely, constant stress and constant strain. The numerical results of both analyses are exactly the same. The reason will be discussed in Section 3.2.3.

3.2.1 CONSTANT STRESS ANALYSIS

Under transverse tension, the local transverse stress, σ_y, is the same for each small volume element situated between y and $y + dy$ as shown in Figure 3(a). It

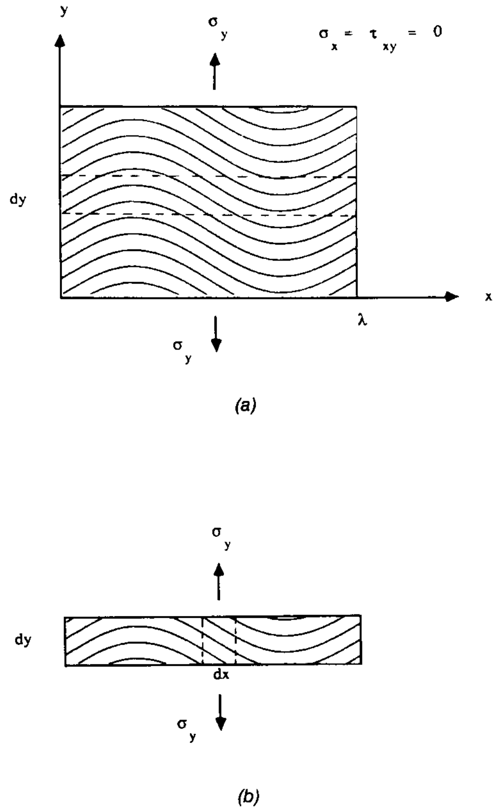

Figure 3. *Iso-phase model under uniform transverse stress,* σ_y.

is assumed that the stress σ_y is uniformly distributed along one wavelength λ [Figure 3(b)]. The small element *dx-dy* in Figure 3(b) is treated as an off-axis unidirectional lamina. By the use of Equation (6) and the plane stress condition, the strain components developed in this element are

$$e_x = \overline{S}_{12}\sigma_y, \qquad e_y = \overline{S}_{22}\sigma_y, \qquad \gamma_{xy} = \overline{S}_{26}\sigma_y \tag{12}$$

The average transverse strain is obtained by averaging the transverse strain, e_y, from $x = 0$ to λ.

$$\overline{e}_y = \frac{1}{\lambda}\int_0^\lambda e_y dx \tag{13}$$

The effective Young's modulus of the iso-phase model in the y direction is

$$E_y^* = \frac{\sigma_y}{\bar{e}_y} = \frac{(1 + c)^{3/2}}{\left[(1 + c)^{3/2} - 1 - \frac{3}{2}c\right]S_{11} + \left(1 + \frac{c}{2}\right)S_{22} + \frac{c}{2}(2S_{12} + S_{66})} \tag{14}$$

The average longitudinal strain, $\bar{e}_x$, is obtained by averaging the longitudinal strain, e_x, from $x = 0$ to λ.

$$\bar{e}_x = \left\{ S_{12} + \left[\frac{c}{2(1 + c)^{3/2}}\right](S_{11} - 2S_{12} + S_{22} - S_{66}) \right\} \sigma_y \tag{15}$$

Also, the average tensile strain along the fibers is obtained by substituting Equation (12) into Equation (8), treating σ_y as a constant, and averaging over the length s.

$$\bar{e}_L = \{(S_{12} - S_{11})F(k) + S_{11}\}\sigma_y \tag{16}$$

where $F(k)$ is defined by Equation (11).

3.2.2 CONSTANT STRAIN ANALYSIS

It was observed in the experiments that when applying a transverse load along the y direction, the elongation of the specimen was uniform throughout its width (Figure 4) away from the specimen ends. This observation motivated us to also

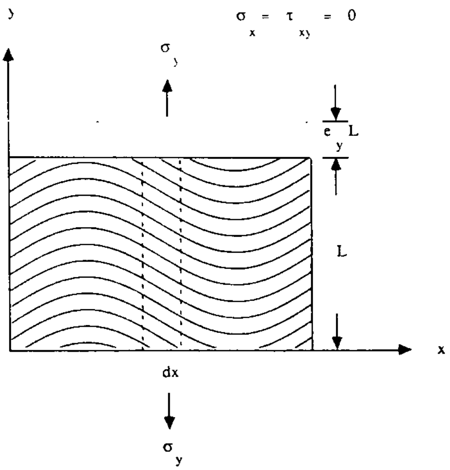

Figure 4. *Iso-phase model under uniform transverse strain, e_y.*

conduct the analysis based upon the constant strain assumption. Since a plane stress condition is assumed, Equation (12) is still valid for the strain components in the small element of width dx. For the constant transverse strain e_y, the induced transverse stress σ_y in each element is obtained from Equation (12).

$$\sigma_y = \frac{1}{\bar{S}_{22}} e_y \tag{17}$$

The average transverse stress is obtained by averaging the transverse stress, σ_y, from $x = 0$ to λ.

$$\bar{\sigma}_y = \frac{1}{\lambda} \int_0^\lambda \sigma_y dx \tag{18}$$

The effective Young's modulus of the iso-phase model in the y direction is

$$\begin{aligned} E_y^* &= \frac{\bar{\sigma}_y}{e_y} \\ &= \frac{1}{S_{11}} - \frac{A}{2c^2 S_{11}} (\alpha - \beta) \end{aligned} \tag{19}$$

where

$$\alpha = \frac{(c\xi + 4)^2}{(R_1 - R_2)} \qquad \beta = \frac{(c\eta + 4)^2}{(R'_1 - R'_2)}$$

$$\xi = \frac{(R_1 + 1)^2}{R_1} \qquad \eta = \frac{(R'_1 + 1)^2}{R'_1}$$

$$R_1 = U_2 + \sqrt{U_2^2 - 1} \qquad R_2 = U_2 - \sqrt{U_2^2 - 1}$$

$$R'_1 = U_1 + \sqrt{U_1^2 - 1} \qquad R'_2 = U_1 - \sqrt{U_1^2 - 1}$$

$$A = \frac{1}{U_1 - U_2} \tag{20}$$

$$U_1 = -1 + \frac{-(2S_{12} + S_{66}) + \sqrt{(2S_{12} + S_{66})^2 - 4S_{11}S_{22}}}{cS_{11}}$$

$$U_2 = -1 + \frac{-(2S_{12} + S_{66}) - \sqrt{(2S_{12} + S_{66})^2 - 4S_{11}S_{22}}}{cS_{11}}$$

The average longitudinal strain, $\bar{e}_x$, is obtained by averaging the longitudinal strain, e_x, from $x = 0$ to λ.

$$\bar{e}_x = \left\{ \frac{S_{12}}{S_{11}} - \frac{A}{2c^2 S_{11}} \left[S_{12}(\alpha - \beta) + 4(S_{11} + S_{22} - S_{66}) \left(\frac{\xi}{R_1 - R_2} - \frac{\eta}{R'_1 - R'_2} \right) \right] \right\} e_y \tag{21}$$

where α, β, ξ, η, R_i, and R'_i ($i = 1,2$) are defined in Equation (20). Also, the average tensile strain along the fibers is obtained by substituting Equation (12)

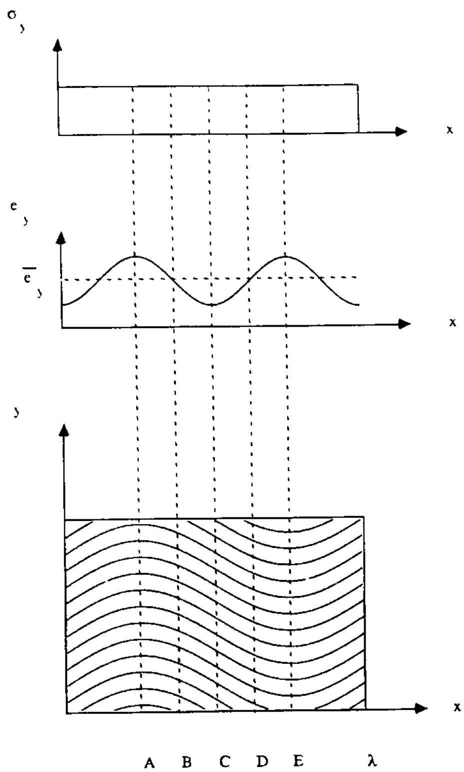

Figure 5. Schematic diagram for constant stress analysis.

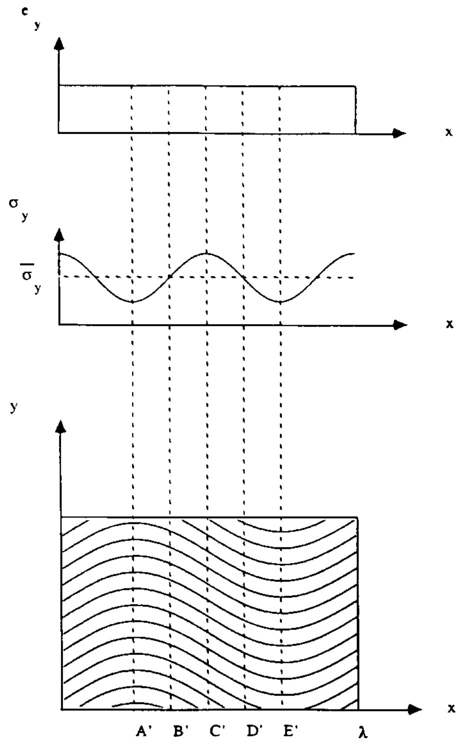

Figure 6. *Schematic diagram for constant strain analysis.*

into Equation (8), treating e_y as a constant, and averaging over the length s.

$$\bar{e}_L = \frac{\lambda e_y}{\pi s} \int_{-1}^{1} G(u) \frac{du}{\sqrt{1 - u^2}} \tag{22}$$

where

$$G(u) = \frac{\left[\frac{c}{2}(u + 1)S_{11} + S_{12}\right]\left[1 + \frac{c}{2}(u + 1)\right]^{3/2}}{\left[\frac{c}{2}(u + 1)\right]^2 S_{11} + \frac{c}{2}(u + 1)(2S_{12} + S_{66}) + S_{22}} \tag{23}$$

3.2.3 COMPARISON OF CONSTANT STRESS AND CONSTANT STRAIN ANALYSES

Consider a specimen of width λ. Figure 5 shows the configuration of deformation for the constant stress analysis. Based on the constant stress assumption, the transverse strain is different in each small volume element and depends on the fiber orientation. Volume elements in the vicinities of sections A and E with 0° fiber orientation are more readily deformed than that at section C, with fiber orientation of θ_{max}. Thus, the strains at sections B and D may be close to the average strain $\bar{e}_y$. Similarly, Figure 6 shows the deformation configuration for the constant strain analysis. Under the uniformly applied strain, among all the vertical sections in Figure 6, A′ and E′ are the easiest to be deformed, whereas section C′ offers the most resistance to deformation. The average stress $\bar{\sigma}_y$ should occur at sections B′ and D′. Since the fibers are sinusoidal in shape, the stress diagram of the constant strain analysis, and the strain diagram of the constant stress analysis are both sinusoidal with the same wavelength $\lambda/2$. The locations of B and B′ sections (or D and D′) are the same for the two analyses. This means that both analyses deal with the identical material (same fiber orientation) for the stress-strain behavior. Although the constitutive relations are not of the same form, the results should be the same for both analyses. Thus, when the stress (or strain) is considered in the average sense along the x direction, it is expected that these two approaches should yield identical predictions. The numerical calculations indeed give the same results.

4. RANDOM-PHASE MODEL

The random-phase model [11] is depicted in Figure 7; the orientation, θ, of fibers at each x cross-section is randomly distributed. As a result, the stretching-shear coupling, existing in the iso-phase model, could be eliminated through the random positioning of curved fibers along the x direction. The spatial position of curved fibers in the xyz coordinates in the xy plane is given by

$$y = a \sin\left[\frac{2\pi}{\lambda}(x - d)\right] \tag{24}$$

where d is the translation of the sinusoidally shaped fiber in the x direction. A

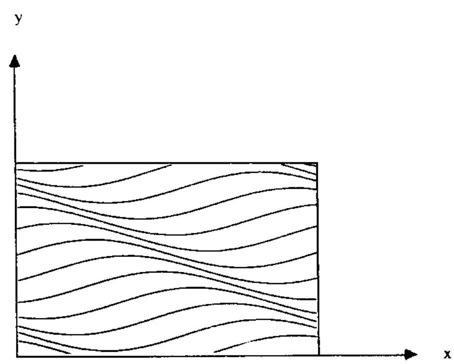

Figure 7. Random-phase model [11].

random distribution of d ($0 \leq d \leq \lambda$) is assumed in the random-phase model. That is, in each infinitesimal section dx, fibers with any arbitrary orientation exist with the same probability. Therefore, it is assumed that the strains e_x and e_y are uniform throughout the domain under longitudinal or transverse tension, and the stress in a fiber segment depends on its orientation, θ.

$$-\frac{2\pi a}{\lambda} \leq \tan\theta \leq \frac{2\pi a}{\lambda} \tag{25}$$

By these assumptions, the classical laminated plate theory can be applied again.

The constitutive relations of an off-axis unidirectional lamina with fiber orientation θ in the xy plane are also given by [14]

$$\begin{Bmatrix} \sigma_x \\ \sigma_y \\ \tau_{xy} \end{Bmatrix} = \begin{bmatrix} \bar{Q}_{11} & \bar{Q}_{12} & \bar{Q}_{16} \\ \bar{Q}_{12} & \bar{Q}_{22} & \bar{Q}_{26} \\ \bar{Q}_{16} & \bar{Q}_{26} & \bar{Q}_{66} \end{bmatrix} \begin{Bmatrix} e_x \\ e_y \\ \gamma_{xy} \end{Bmatrix} \tag{26}$$

where

$$\begin{aligned}
\bar{Q}_{11} &= Q_{11}\cos^4\theta + Q_{22}\sin^4\theta + 2(Q_{12} + 2Q_{66})\sin^2\theta\cos^2\theta \\
\bar{Q}_{12} &= Q_{12} + (Q_{11} - 2Q_{12} + Q_{22} - 4Q_{66})\sin^2\theta\cos^2\theta \\
\bar{Q}_{22} &= Q_{11}\sin^4\theta + Q_{22}\cos^4\theta + 2(Q_{12} + 2Q_{66})\sin^2\theta\cos^2\theta \\
\bar{Q}_{16} &= (Q_{11} - Q_{12} - 2Q_{66})\cos^3\theta\sin\theta + (Q_{12} - Q_{22} + 2Q_{66})\cos\theta\sin^3\theta \\
\bar{Q}_{26} &= (Q_{11} - Q_{12} - 2Q_{66})\cos\theta\sin^3\theta + (Q_{12} - Q_{22} + 2Q_{66})\cos^3\theta\sin\theta \\
\bar{Q}_{66} &= (Q_{11} - 2Q_{12} + Q_{22} - 4Q_{66})\sin^2\theta\cos^2\theta + Q_{66}
\end{aligned} \tag{27}$$

Q_{11}, Q_{22}, Q_{12} and Q_{66} are the elastic stiffness constants of the unidirectional lamina.

The small volume element situated between x and $x + dx$ is treated as a laminate composed of many unidirectional laminae with different fiber orientations. The fibers with the orientation, θ, have the probability dx/λ, and lie in the range defined by

$$\frac{2\pi a}{\lambda}\cos\frac{2\pi x}{\lambda} \leq \tan\theta \leq \frac{2\pi a}{\lambda}\cos\frac{2\pi(x + dx)}{\lambda} \tag{28}$$

Therefore, the stress-strain relation of the laminate can be rewritten as

$$\begin{Bmatrix} \sigma_x \\ \sigma_y \\ \tau_{xy} \end{Bmatrix} = \begin{bmatrix} C_{11} & C_{12} & C_{16} \\ C_{12} & C_{22} & C_{26} \\ C_{16} & C_{26} & C_{66} \end{bmatrix} \begin{Bmatrix} e_x \\ e_y \\ \gamma_{xy} \end{Bmatrix} \tag{29}$$

where

$$C_{mn} = \frac{1}{\lambda}\int_0^{\lambda} \overline{Q}_{mn}(\theta)dx \tag{30}$$

The average stiffness constants are [11]

$$\begin{aligned}
C_{11} &= \frac{1}{(1+c)^{3/2}}\left\{Q_{11}\left(1+\frac{c}{2}\right) + (Q_{12}+2Q_{66})c \right.\\
&\quad \left. + Q_{22}\left[(1+c)^{3/2} - \left(1+\frac{3}{2}c\right)\right]\right\}\\
C_{22} &= \frac{1}{(1+c)^{3/2}}\left\{Q_{11}\left[(1+c)^{3/2} - \left(1+\frac{3}{2}c\right)\right]\right.\\
&\quad \left. + (Q_{12}+2Q_{66})c + Q_{22}\left(1+\frac{c}{2}\right)\right\}\\
C_{12} &= \frac{1}{(1+c)^{3/2}}\left\{(Q_{11}+Q_{22}-4Q_{66})\frac{c}{2} + Q_{12}[(1+c)^{3/2} - c]\right\}\\
C_{66} &= \frac{1}{(1+c)^{3/2}}\left\{(Q_{11}+Q_{22}-2Q_{12})\frac{c}{2} + Q_{66}[(1+c)^{3/2} - 2c]\right\}\\
C_{16} &= 0\\
C_{26} &= 0
\end{aligned} \tag{31}$$

Now the stretching-shear coupling has been eliminated; $C_{16} = C_{26} = 0$. Equation (29) leads to

$$\begin{Bmatrix} e_x \\ e_y \\ \gamma_{xy} \end{Bmatrix} = \begin{bmatrix} S_{11}^* & S_{12}^* & 0 \\ S_{12}^* & S_{22}^* & 0 \\ 0 & 0 & S_{66}^* \end{bmatrix} \begin{Bmatrix} \sigma_x \\ \sigma_y \\ \tau_{xy} \end{Bmatrix} \tag{32}$$

where the average compliant constants are

$$\begin{aligned}
S_{11}^* &= C_{22}C_{66}/D\\
S_{22}^* &= C_{11}C_{66}/D\\
S_{12}^* &= -C_{12}C_{66}/D\\
S_{66}^* &= (C_{11}C_{22} - C_{12}^2)/D\\
D &= C_{11}C_{22}C_{66} - C_{12}^2C_{66}
\end{aligned} \tag{33}$$

4.1 Longitudinal Young's Modulus

The longitudinal Young's modulus and major Poisson's ratio [11] of the random-phase composite are

$$E_x^* = \frac{1}{S_{11}^*}, \qquad \nu_{xy}^* = -\frac{S_{12}^*}{S_{11}^*} \tag{34}$$

If the random-phase model is subjected to uniaxial tension, σ_x, the strain components are given by

$$e_x = \frac{1}{E_x^*}\sigma_x, \qquad e_y = -\frac{\nu_{xy}^*}{E_x^*}\sigma_x, \qquad \gamma_{xy} = 0 \tag{35}$$

The average tensile strain along the fibers is obtained by substituting Equation (35) into Equation (8) and averaging through s.

$$\bar{e}_L = (e_x - e_y)F(k) + e_y \tag{36}$$

where $F(k)$ is given by Equation (11).

4.2 Transverse Young's Modulus

The transverse Young's modulus and minor Poisson's ratio are given by

$$E_y^* = \frac{1}{S_{22}^*}, \qquad \nu_{yx}^* = -\frac{S_{12}^*}{S_{22}^*} \tag{37}$$

When the random-phase composite is subjected to transverse stress, σ_y, the strain components are given by

$$e_x = -\frac{\nu_{yx}^*}{E_y^*}\sigma_y, \qquad e_y = \frac{1}{E_y^*}\sigma_y, \qquad \gamma_{xy} = 0 \tag{38}$$

The average tensile strain along the fibers is obtained by substituting Equation (38) into Equation (8) and averaging through s.

$$\bar{e}_L = (e_x - e_y)F(k) + e_y \tag{39}$$

where $F(k)$ is given by Equation (11).

5. EXPERIMENTS

5.1 Materials

In order to study the nonlinear elastic behavior under large deformation, the flexible composite specimens with curved fibers in an elastomeric matrix were

Table 1. Elastic constants of SYLGARD 184 silicone elastomer [13].

Initial Young's Modulus $E°$ (MPa)	1.7
Shear rigidity G (MPa)	0.582*
Poisson's ratio ν	0.46
Maximum breaking strain e_b (%)	50–100

*Isotropic relation $G = E/2(1 + \nu)$ is assumed.

fabricated. SYLGARD 184 silicone elastomer used as matrix material in the experiments is supplied by Dow Corning Company [3]. It exhibits nearly perfect elastic behavior [2] and the plastic strain upon unloading is no greater than 0.15%. Maximum elongation is up to 100%. It remains transparent after curing. Tensile experiments of pure silicone elastomer specimens are performed to determine the elastic constants, which are shown in Table 1 [13].

For the photoelastic experiments, photostress coating material PL-3 is chosen as the matrix material because it can sustain large elongation and has good photoelastic characteristics. This epoxy resin based material is mixed with the hardener material PLH-3. Both PL-3 and PLH-3 are supplied by Measurements Group, Inc. The ratio of hardener to resin is 150 pph (parts per hardener) by weight.

Carbon fibers are chosen for good contrast between the fiber and matrix and hence, ease of observations as discussed in Reference [3]. The carbon fibers used for fabricating the specimens are Thornel-300, supplied by Union Carbide. A loose fiber bundle contains 1000 filaments with a filament diameter of 7 μm. Their elastic constants are shown in Table 2 [15].

5.2 Fabrication Method

5.2.1 CURVED FIBER

The fiber yarns are carefully wound onto a plastic frame without being twisted. The aligned yarns are wetted in SYLGARD prime coat liquid (supplied by Dow Corning Company) for the purpose of enhancing the adhesion to the matrix. A mold (12″ × 3″) is used to press the yarns into the desired sinusoidal shape. The two matching halves of the mold, made of Delrin AF polyacetal, have a sinusoidal wavy surface with amplitude, $a = 6/100″$, and wavelength, $\lambda = 2/3″$.

Table 2. Elastic constants of Thornel-300 carbon fiber [15].

E_L (GPa)	225
E_T (GPa)	20.54
G_{LT} (GPa)	41.16
ν_{LT}	0.31
ν_{TT}	0.33
e_b (%)	3

The molds are removed after 24 hours, and the curved fibers are obtained. The theoretical a/λ ratio is 0.09. Actually, the a/λ ratio varied from specimen to specimen.

5.2.2 SPECIMEN FABRICATION

The specimen size was 1.5″ × 9″ for both longitudinal and transverse tensile tests. An aluminum casting plate (6/100″ in thickness) with a cavity of the size of the specimen is used as the mold. A thin Teflon sheet is placed underneath the plate. A piece of paper with the desired fiber arrangement drawn on it is placed under the Teflon film. The seal between the plate and Teflon film prevents seepage of the matrix resin.

A measured amount of resin is first poured into the opening of the casting plate so as to reach half of the plate thickness. This layer of resin becomes very sticky after being kept at room temperature for 16 hours, and the fiber placement process begins. The position of the fibers is determined by the graph paper under the Teflon film. After the fibers have been aligned, resin matrix is filled up to the plate thickness. This assembly is kept at room temperature for 24 hours, and then covered by another thin Teflon film, and placed in an autoclave for curing. After curing the Teflon films are peeled off from the specimens prior to testing. Since it takes time for the resin to wet the fiber bundles thoroughly, keeping the specimens at room temperature for 24 hours is a very crucial step; putting the specimens into the autoclave too early would produce a lot of air bubbles. Vacuuming of the specimen assembly is effective in removing the air bubbles [2].

5.3 Experimental Methods

Two kinds of experiments were conducted to verify the constitutive relations: photoelastic and tensile tests.

5.3.1 PHOTOELASTIC TEST

In order to study the microscopic stress distribution, longitudinal tensile photoelastic tests were conducted for the iso-phase specimens. The deformation of specimens was observed using a transmission polariscope. The photoelastic color sequence varied with increasing stress as follows: black, red and blue-green, red and green, red and dark green [16]. The yellow color presents at the transition from one stress level to another.

By the color print [1], the color sequence observed from the section with zero degree fiber orientation to the section with θ_{max} fiber orientation is yellow, red and blue-green, yellow, red and green, and symmetrical about the half wavelength. Although Figure 8 does not show the color sequence, the relative rotation of the dark fringes indicates maximum shear deformation of the matrix at the sections with fiber orientation of θ_{max}, and the white fringes indicate minimum shear deformation at the sections with 0° fiber orientation. Since the fibers bear the most part of the load at the section with 0° fiber orientation, the matrix experiences the least stress. At the section with fiber orientation of θ_{max}, the matrix

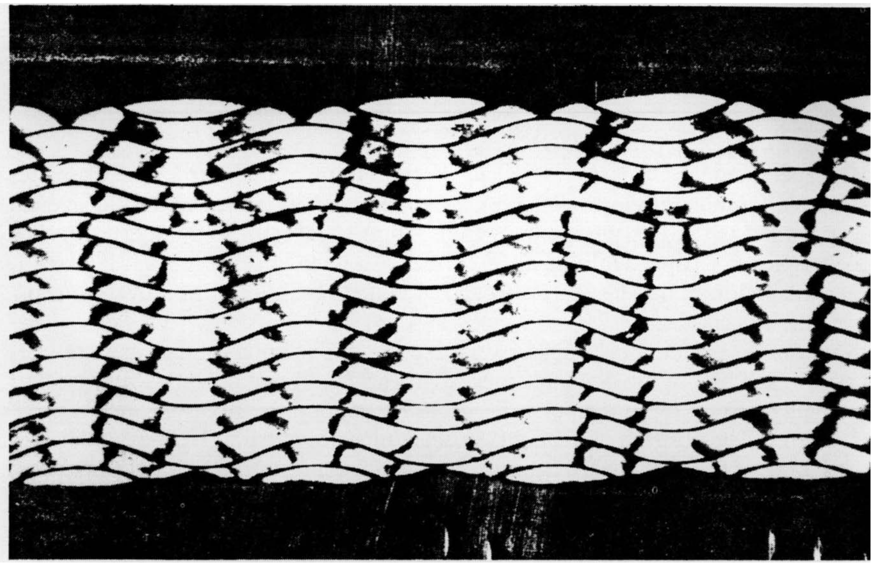

Figure 8. *Longitudinal tensile photoelastic test of iso-phase model [3,12].*

experiences more stress than any other sections. Failure of the composite initiates in the matrix or at the fiber/matrix interface at sections of θ_{max} in fiber orientation due to concentration of shear deformation.

5.3.2 TENSILE TEST

All the tensile tests were conducted on an Instron machine (model 1125). The cross head speeds employed were 0.2 in/min and 0.5 in/min for longitudinal and transverse tensile tests, respectively. A 1000 lb load cell was used to measure the load in all the tests.

As mentioned earlier, the deformation of flexible composites is very non-uniform. The way to determine the strain is to average it over a characteristic length of the specimen. For longitudinal tests, this length is determined from the fiber wavelength whereas for the transverse tests, it is determined from the fiber spacing. Prior to testing, lines were drawn on the specimens to mark these characteristic lengths. The lengths chosen for the longitudinal and transverse tests were 2 in (three fiber wavelengths) and 3/4 in (eleven fiber spacings), respectively.

Photographs of the specimens were taken for each increment in strain. Because stress relaxation occurs in the elastomeric materials, the photos were taken at 5 seconds delay after stopping the Instron. The length between the markings was directly measured by a vernier caliper from the enlarged projection of the negatives created by an enlarger in a dark room.

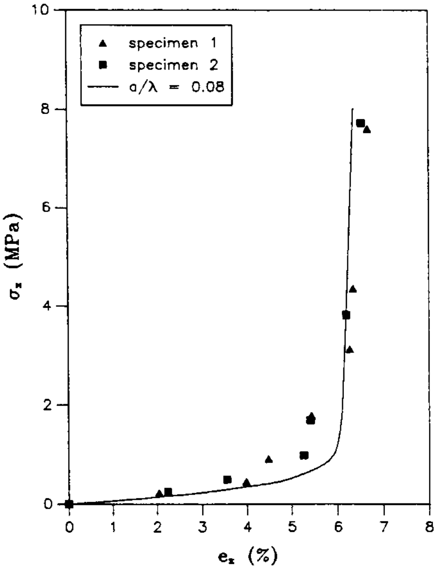

Figure 9. *Comparison between the theoretical curve and experimental data of longitudinal tension, iso-phase model. Initial of the tensile specimens a/λ ≈ 0.07 ~ 0.09, and V_f = 1.18%.*

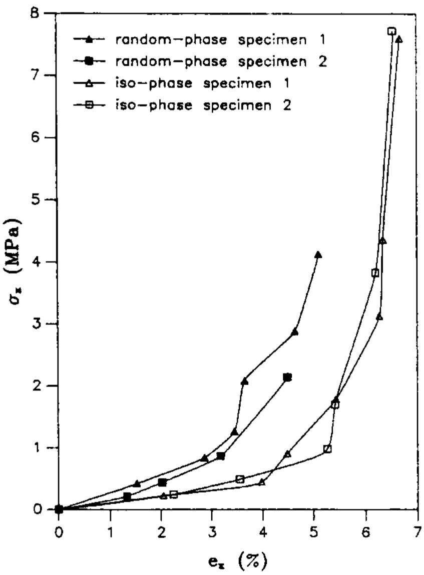

Figure 10. *Comparison between iso-phase and random-phase models, experimental data of longitudinal tension.*

6. RESULTS

The prediction of the nonlinear behavior is based on the constitutive relations derived in Sections 2, 3 and 4. For numerical calculation, the nonlinear stress-strain response of flexible composites is examined by applying the incremental analysis to take into account the change of fiber shape and rubber elasticity as presented by Chou and Takahashi [11]. The true strain, ϵ, is obtained by the incremental analysis. In the following comparisons, the engineering strain, e, is used which is converted from the true strain, ϵ.

The fiber volume fraction and initial a/λ ratio vary slightly from specimen to specimen. The average value of fiber volume fraction is used in the theoretical prediction.

6.1 Longitudinal Tensile Test

Figure 9 shows the results of longitudinal tensile test on iso-phase specimens. The average a/λ value measured from the specimens is about 0.08. Figure 10 gives the comparison of experimental data between iso-phase and random-phase models. The random-phase specimens give higher stiffness than that of the iso-phase model as predicted by Chou and Takahashi [11].

6.2 Transverse Tensile Test

Figures 11 and 12 show the transverse tensile results of the iso-phase and

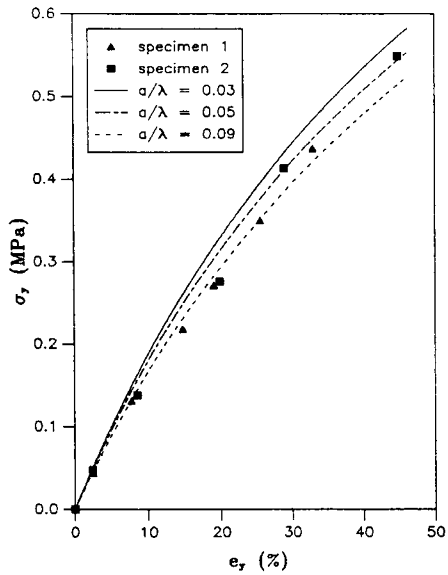

***Figure 11.** Comparison between theoretical curves and experimental data of transverse tension, iso-phase model. Initial of the tensile specimen $a/\lambda \approx 0.05 \sim 0.07$, and $V_f = 1.337\%$.*

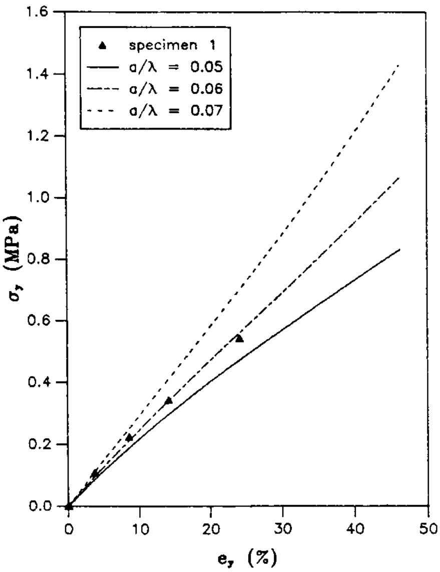

Figure 12. *Comparison between theoretical curves and experimental data of transverse tension, random-phase model. Initial of the tensile specimen a/λ ≈ 0.05 ~ 0.07, and $V_f = 1.263\%$.*

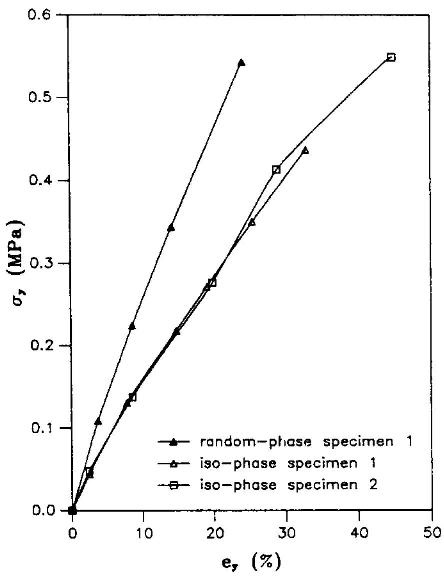

Figure 13. *Comparison between iso-phase and random-phase models, experimental data of transverse tension.*

random-phase models, respectively. For the iso-phase specimens, the average measured value of initial a/λ ratio is about 0.05; the theoretical curves fit the experimental data very well. The theoretical curves are relatively insensitive to the initial a/λ ratio for the iso-phase model, but sensitive to the initial a/λ ratio for the random-phase model. Although the random-phase specimens are not ideal, the experimental data and theoretical curves coincide very well. It was observed in the experiment that the marked lines remain straight after deformation, indicating that the uniform strain assumption is valid for the random-phase specimens. Figure 13 shows that the transverse stiffness of the random-phase model is also higher than that of the iso-phase model.

7. CONCLUSIONS

1. Constitutive relations for the longitudinal and transverse tensile behavior have been developed for flexible composites. The flexible composites examined in this research are composed of continuous fibers with sinusoidal waviness in an elastomeric matrix. Two types of fiber arrangement are considered for both theoretical and experimental studies, namely, iso-phase and random-phase models.
2. In the longitudinal tensile tests, the results compare very well with the theoretical predictions for the iso-phase model.
3. In the transverse tensile case, both constant stress and constant strain analyses are performed for the iso-phase model. In spite of the different assumptions, the predictions are the same for both analyses. The stiffness of the matrix dominates the nonlinear transverse stress-strain behavior of the flexible composites. Experimental results show good agreement with the theoretical predictions for both iso-phase and random-phase models. Experimental observations indicate that the uniform strain condition is valid for both iso-phase and random-phase specimens.

ACKNOWLEDGEMENTS

This research was partially supported by the National Science Foundation through the Center for Composites Manufacturing Science and Engineering of University of Delaware. Special thanks are due to Professor David M. Barnett at Stanford University for valuable discussions and providing computer facilities to the first author.

REFERENCES

1. Chou, T.-W., R. L. McCullough and R. B. Pipes. "Composites," *Scientific American*, 254:192–203 (1986).
2. Luo, S.-Y. "Nonlinear Elastic Behavior of Flexible Composites," M.S. Thesis, University of Delaware (June 1986).
3. Lou, S.-Y. and T.-W. Chou. "Modeling of Nonlinear Elastic Behavior of Elastomeric Flexible Composites," *Abstracts of The 192nd National Meeting of the American Chemical Society* (September 1986).
4. Ishikawa, T. and T.-W. Chou. "Elastic Behavior of Woven Hybrid Composites," *Journal of Composite Materials*, 16:2–19 (1982).

5. Ishikawa, T. and T.-W. Chou. "One-Dimensional Micromechanical Analysis of Woven Fabric Composites," *AIAA Journal*, 21:1714–1721 (1983).
6. Ishikawa, T. and T.-W. Chou. "Stiffness and Strength Behavior of Woven Fabric Composites," *Journal of Materials Science*, 17:3211–3220 (1982).
7. Ishikawa, T. and T.-W. Chou. "Nonlinear Behavior of Woven Fabric Composites," *Journal of Composite Materials*, 17:399–413 (1983).
8. Yang, J.-M., C.-L. Ma and T.-W. Chou. "Elastic Stiffness of Biaxial and Triaxial Woven Fabric Composites," *Proceedings of the 29th National SAMPE Symposium*, pp. 292–303 (1984).
9. Ma, C.-L., J.-M. Yang and T.-W. Chou. "Elastic Stiffness of Three-Dimensional Braided Textile Structural Composites," *ASTM Symposium on Testing and Design of Composite Materials*, American Society for Testing and Materials, pp. 404–421 (1986).
10. Yang, J.-M., C.-L. Ma and T.-W. Chou. "Fiber Inclination Model of Three-Dimensional Textile Structural Composites," *Journal of Composite Materials*, 20:472–484 (1986).
11. Chou, T.-W. and K. Takahashi. "Nonlinear Elastic Behaviour of Flexible Fibre Composites," *Composites*, 18:25–34 (1987).
12. Luo, S.-Y. and T.-W. Chou. "Finite Deformation and Nonlinear Elastic Behavior of Flexible Composites," accepted for publication in *Journal of Applied Mechanics*, 55:149–155 (1988).
13. Kuo, C.-M. "Nonlinear Elastic Behavior of Flexible Composites," M.S. Thesis, University of Delaware (December 1986).
14. Vinson, J. R. and T.-W. Chou. *Composite Materials and Their Use in Structures*, Slsevier-Applied Science, London (1975).
15. Chi, Z. and T.-W. Chou. "An Experimental Study of the Effect of Prestressed Loose Carbon Strands on Composite Strength," *Journal of Composite Materials*, 17:196–209 (1983).
16. Instruction Bulletin SFC-300, Measurements Group, INC.